The N-Terminal Domain of Human Centrin 2 Has a Closed Structure, Binds Calcium with a Very Low Affinity, and Plays a Role in the Protein Self-Assembly[†,‡]

Ao Yang, Simona Miron, Patricia Duchambon, Liliane Assairi, Yves Blouquit, and Constantin T. Craescu*

INSERM/Institut Curie-Recherche, Centre Universitaire Paris-Sud, Bâtiment 112, 91405 Orsay Cedex, France

Received July 18, 2005; Revised Manuscript Received October 12, 2005

ABSTRACT: Centrins are well-conserved calcium binding proteins from the EF-hand superfamily implicated in various cellular functions, such as centrosome duplication, DNA repair, and nuclear mRNA export. The intrinsic molecular flexibility and the self-association tendency make difficult the structural characterization of the integral protein. In this paper we report the solution structure, the Ca^{2+} binding properties, and the intermolecular interactions of the N-terminal domain of two human centrin isoforms, HsCen1 and HsCen2. In the absence of Ca^{2+}, the N-terminal construct of HsCen2 revealed a compact core conformation including four almost antiparallel α-helices and a short antiparallel *β*-sheet, very similar to the apo state structure of other calcium regulatory EF-hand domains. The first 25 residues show a highly irregular and dynamic structure. The three-dimensional model for the N-terminal domain of HsCen1, based on the high sequence conservation and NMR spectroscopic data, shows very close structural properties. Ca^{2+} titration of the apo-N-terminal domain of HsCen1 and HsCen2, monitored by NMR spectroscopy, revealed a very weak affinity (10^2-10^3 M^{-1}), suggesting that the cellular role of this domain is not calcium dependent. Isothermal calorimetric titrations showed that an 18-residue peptide, derived from the N-terminal unstructured fragment, has a significant affinity ($\sim 10^5$ M^{-1}) for the isolated C-terminal domain, suggesting an active role in the self-assembly of centrin molecules.

Centrins are small size (∼20 kDa) calcium binding proteins from the EF-hand superfamily (also named calmodulin superfamily), well-conserved in the eukaryote kingdom from yeast to humans. The centrin family is continuously increasing since the discovery of its first member in the basal bodies of the green algae *Tetraselmis striata* more than 20 years ago (*1*). These proteins are most concentrated, and therefore easier to observe, in basal bodies of flagellated or ciliated cells, in the spindle pole body (SPB) of yeast cells, and in centrosomes of higher eukaryotes (*1*−*3*). The common function of the basal bodies, SPBs, and centrosomes is related to the nucleation and organization of the microtubule network, in particular during the cell mitosis. Genetic and cell biology experiments demonstrated that the centrosomal fraction of centrins is critically involved in the duplication of these organelles and the proper cellular mitosis (*4, 5*). As a component of Ca^{2+}-sensitive contractile fibers connecting basal bodies and other cell compartments, centrins were also proposed to play a dynamic structural role in basal body morphology (*6, 7*) and in microtubule severing (*8*).

Accumulating evidence demonstrates that the localization of centrins is not limited to centrosomes (*3*) but is related to other cell compartments like the nucleus or the perimembrane space. In addition, new functional implications were recently discovered, including the nuclear DNA repair process (*9*), nuclear transmembrane mRNA export (*10*), or the activity of voltage-gated Ca^{2+} channels in *Paramecium* (*11*).

There are three centrin isoforms in humans (HsCen1 to HsCen3)[1] (*12*). Comparative sequence analysis revealed the existence of two divergent subfamilies: HsCen1, HsCen2, and centrin from *Chlamydomonas* (CrCen) belong to one branch, while HsCen3 and the yeast homologue Cdc31p belong to another branch. Thus, HsCen3 exhibits 54% sequence identity with HsCen1 and HsCen2, while these latter isoforms show 84% sequence identity among them. Sequence analysis and the available experimental data suggested that centrins are organized into two structurally independent domains that could be expressed and studied separately (*13, 14*). It is worth noting that the sequence of the N-terminal domain is significantly less conserved than that of the C-terminal domain (76% and 95%, respectively, for the couple HsCen1/HsCen2). A large contribution to the sequence variability among various centrins originates from the first 20-residue fragment, including many basic side chains (Figure 1). The length, sequence, and basic character of this N-terminal fragment constitute distinctive features

[†] This work was supported by the Institut Curie, the Institut National pour la Santé et la Recherche Médicale, and the Centre National de la Recherche Scientifique.

[‡] The coordinates of the final best 20 structures and the NMR restraint file used in the structure calculations were deposited with the RCSB Protein Data Bank under accession code 1ZMZ.

* To whom correspondence should be addressed. Tel: 33 1 69 86 31 63. Fax: 33 1 69 07 53 27. E-mail: Gil.Craescu@curie.u-psud.fr.

[1] Abbreviations: HsCen1 to HsCen3, human centrin isoforms 1 to 3; N-HsCen1, N-terminal domain (1−97) of HsCen1; N-HsCen2, N-terminal domain (1−98) of HsCen2; C-HsCen2, C-terminal domain of HsCen2 (94−172); CrCen, *Chlamydomonas reinhardtii* centrin; CaM, calmodulin; TnC, troponin C; CaVP, calcium vector protein; ITC, isothermal titration calorimetry; CD, circular dichroism; SDS−PAGE, sodium dodecyl sulfate−polyacrylamide gel electrophoresis.

10.1021/bi051397s CCC: $33.50
Published on Web 12/27/2005

FIGURE 1: Sequence comparison of the N-terminal domains of HsCen1, HsCen2, HsCen3, CrCen, and CaM. The residues involved in calcium binding are shown in red, and the basic side chains in the N-terminal fragment are colored in green. The boxes indicate the conserved Lys and Arg side chains contributing to the positive patch on the protein-exposed surface. The N-18 peptide used in binding studies corresponds to the underlined sequence. The sequence number and the secondary structure elements corresponding to N-HsCen2 are reported on the top of the figure.

among the members of the large CaM superfamily. In the case of human isoforms HsCen1 and HsCen2, the N-terminal half exhibits an additional specific property: it has a higher pH_i value (7.93 and 7.91, respectively), relative to the usual EF-hand domains (pH_i between 4.0 and 4.5).

Elucidating the structural basis for the cellular activity of centrins, including target selectivity, binding mode, and biological activation, requires a deeper insight into their structural and molecular characteristics. The biochemical and biophysical data obtained so far were based on the study of integral proteins (*15*, *16*) and isolated EF-hand domains (*13*, *14*, *17*). Studies on HsCen2 (*14*) and CrCen (*13*) showed that the C-terminal domain is poorly structured in the absence of Ca^{2+} and that the metal binding produces conformational changes and stabilizes the structure. Unfortunately, even at higher calcium-to-protein ratios, the structure of this domain is still very flexible and explores multiple conformations, precluding the structure determination either by NMR or by X-ray crystallography. High-affinity interactions with peptides derived from potential centrin targets, like XPC (*17*) or Kar1 (*18*), result in stable bimolecular complexes with a unique and persistent structure. It is therefore inferred that this half of the molecule is determinant for the cellular regulatory role. Much less is known on the biological role of the N-terminal half of centrins.

The localization, affinity, and selectivity for divalent cations are quite different among the various studied centrins (*13*, *14*, *16*). Thus, HsCen2 has a unique high-affinity binding site localized in binding loop IV (*14*), while CrCen shows four significant binding sites, the strongest being localized in the N-terminal domain (*13*). HsCen3 revealed a different binding behavior: it has three Ca^{2+} binding sites, one of them, situated in the N-terminal domain, being a mixed Ca^{2+}/Mg^{2+} site (*19*). The variable metal binding capacity of the centrins' N-terminal domain raises the question of the role that this domain may play in the biological functions of various centrins. To address this question, we initiated the study of conformational and molecular properties of the isolated domains from HsCen1 and HsCen2 and explored their metal and protein binding properties. The results reported in this paper demonstrate that the N-terminal half has a compact closed structure in solution, similar to the apo conformation of representative EF-hand domains studied so far. As the measured calcium affinity is much lower relative to the intracellular concentration of the metal ion, this conformation is relevant for the cell state of HsCen1 and HsCen2. Calorimetric measurements revealed that the first 25-residue fragment, which has no persistent structure, may bind to the C-terminal domain dimers, thus contributing to the self-association process of the integral centrins.

MATERIALS AND METHODS

Materials. Sequences coding for residues 1−97 or 1−98 from HsCen1 and HsCen2, respectively, were PCR amplified using plasmids containing the full sequence coding for HsCen2 (*14*) and HsCen1 (pLA11.33.2, constructed using a clone kindly provided by M. Bornens) and the following primers: 5′-N-HsCen2, 5′-ATGGCCTCCAACTTTAAG-3′; 3′-N-HsCen2, 5′-AGACATTTTCTGGGTCATC-3′; 5′-N-HsCen1, 5′-GGAATTCCATATGGCTTCCGGCTTCAAGAAG-3′; 3′-N-HsCen1, 5′-CGGCGCTCGAGTCACATCTTCTGCGTCATCACGGC-3′.

The purified PCR products were cloned into the expression vectors pETBlue (Novagen) at the *Eco*RV restriction sites, giving the plasmid pPD2-2-3 encoding N-HsCen2, and pET24a (Novagen) at the *Eco*RV restriction sites, giving the plasmid pLA11.33.3 encoding N-HsCen1. The resulting plasmids were sequenced in order to verify their integrity and then used to transform the *Escherichia coli* strains Tuner (DE3) pLacI or Bl21(DE3) pDIA17 (*20*). Recombinant strains were grown in a 2YT medium supplemented with appropriate antibiotics at 37 °C, to an absorbance of 1.5 at 600 nm; then the overproduction of the recombinant proteins was induced by the addition of 1 mM isopropyl 1-β-D-thiogalactoside (IPTG), and the growth was continued for an additional 3 h at 37 °C. For ^{15}N-labeled samples, we used the M9 culture medium containing $^{15}NH_4Cl$ (1 g/L) as the sole source of nitrogen, glucose (4 g/L), 2 mM $MgSO_4$, 0.1 mM $CaCl_2$, 3 μM thiamin, 3.6 μM $FeSO_4$, and appropriate antibiotics. The first preculture (10 mL of liquid M9 medium

in a 100 mL shake flask) was inoculated with several colonies from the Petri dish, grown overnight on M9 medium/agar at 37 °C, and incubated at 37 °C for 8−10 h. The second preculture was inoculated with the first preculture (1% v/v), incubated at 37 °C for 12−14 h, and then used to inoculate 2 L of M9 medium, OD 0.1 at 600 nm. Cells were incubated at 37 °C and 160 rpm. When absorbance at 600 nm reached 1.5, 0.1 mM IPTG was added for 18 h at 32 °C to induce the synthesis of the recombinant protein.

The cells were disrupted in a glycerophosphate buffer (50 mM), pH 7.4, containing EDTA (2 mM), NaCl (50 mM), β-mercaptoethanol (2 mM), and an antiprotease cocktail (Complete, Roche), using a 2 kbar cell disrupter (Constant Systems, Warwick, U.K.). After 30 min centrifugation at 20000 *g*, the supernatant was loaded on a DEAE-TSK column, equilibrated with a similar glycerophosphate buffer at pH 8.5, and eluted with a NaCl gradient from 0.05 to 0.25 M. The fractions containing the centrin domain were then deposited on a phenyl-TSK column, equilibrated in glycerophosphate buffer (50 mM), NaCl (0.1 M), and EDTA (5 mM), pH 7.0, that was eluted with ammonium sulfate buffer from 2 to 0 M. The purified samples were concentrated on YM3 Diaflo ultrafiltration membranes (Amicon, Beverly, MA) and desalted on a Sephadex G-25 column equilibrated with NH_4HCO_3 buffer (1.5%). The identity and purity of the samples were checked by SDS−PAGE electrophoresis and mass spectrometry.

The peptide N-18, FKKANMASSSQRKRMSPK from HsCen2, purchased from Biofidal (Vaulx-en-Velin, France), was more than 95% pure.

CD Spectroscopy. CD experiments were performed on a Jasco J-715 CD spectropolarimeter equipped with a Peltier temperature controller. Far-UV spectra were recorded between 190 and 250 nm at 20 °C using 1 mm path length quartz cells. Spectra were collected as an average of five scans, with a scan speed of 20 nm/min and a response time of 2 s. Samples were measured at 10 μM protein concentration, pH 6.6, in 1 mM MOPS buffer and 0.4 mM NaCl. The apo- and holoprotein samples contained 0.25 mM EGTA and 1.4 mM $CaCl_2$, respectively. The buffer signal was digitally subtracted using the software provided by the manufacturer. Thermal denaturation was followed by CD spectroscopy, recording the ellipticity at 222 nm between 5 and 95 °C with a temperature increasing rate of 1 °C/min. Reversibility of the thermal unfolding process was assessed to be higher than 95%, by comparing the CD spectra at the beginning and at the end of the thermal cycle.

NMR Spectroscopy. NMR samples (0.7−1.5 mM) were obtained by dissolving the lyophilized protein in deuterated Tris-HCl buffer (20 mM, pH 6.5) containing 100 mM NaCl. NMR spectra were recorded on a Varian Unity500 NMR spectrometer, equipped with a triple probe and a *Z*-field gradient, at 298 or 308 K. Standard homonuclear 2D experiments (COSY-DQF, TOCSY, NOESY) in ^1H_2O or ^2H_2O were used for the resonance assignment and collection of distance and angle restraints (*21*). Heteronuclear 2D ($^{15}N-^1H$)-HSQC, 3D ($^{15}N-^1H$)-NOESY-HSQC, and ($^{15}N-^1H$)-TOCSY-HSQC spectra were used to assign the ^{15}N resonances as well as to complete the proton assignment and interproton distance restraints. Spectroscopic data analysis was carried out using Felix 2000.1 software (Accelrys, San Diego, CA).

Structure Determination. Interproton distance restraints were obtained from NOESY spectra in ^1H_2O or ^2H_2O with mixing times of 100 and 150 ms. Peak intensities were calibrated relative to NOEs corresponding to known interproton distances such as $H^N(i)-H^N(i+1)$ (2.8 Å in an α-helix) and $H^\beta1(i)-H^\beta2(i)$ (1.8 Å in methylene groups). The NOE restraints were classified into three categories: strong (1.8−3.0 Å), medium (3.0−3.8 Å), and weak (3.8−5.0 Å). Within the segments having a regular secondary structure, the observable distance restraints [$d_{\alpha N}(i,i+2)$, $d_{NN}(i,i+2)$, etc.] were confined to a range (±0.2 Å) around the standard distance characteristic to well-resolved structures (*21*). The final experimental restraints include 1159 NOE-based interproton distances, 36 hydrogen bonds, and 50 dihedral angles (see Table 1). The solution structures were generated using the simulated annealing procedure (*22*), under NMR experimental restraints. In the final run, after the optimization of the restraint file, we generated 200 structures and retained the best 20 structures based on the stereochemical quality, low potential energy, and agreement with the restraint file. The first structure in this assembly, which is closest to the average coordinates of the ensemble, was chosen as a representative conformer and used for structural illustration. The AQUA and PROCHECK-NMR packages (*23*) were used for analysis of secondary structure, side chain conformations, hydrogen bonds, and restraint violations. The electrostatic potential at the molecular surface was calculated and graphically represented using the GRASP software (*24*).

Isothermal Titration Calorimetry. Thermodynamic parameters of intermolecular interactions at constant temperature (35 °C) were investigated by ITC using a MicroCal MCS instrument (MicroCal Inc., Northampton, MA). The samples were equilibrated in the same buffer (usually 50 mM MOPS, pH 6.8, 20 mM NaCl, and 1 mM $CaCl_2$) and degassed before their use. In a standard experiment, one sample (usually 250 μM peptide N18) in a 300 μL syringe is diluted into the 1.337 mL calorimeter cell containing the protein, using automatic injections of 8−15 μL each. Integration of the heat peaks corresponding to each injection and correction for the baseline, performed using Origin-based software, give the enthalpy variation along the mixing path, which represents the reaction isotherm. Fitting the data to an interaction model results in the stoichiometry (n), the equilibrium binding constant (K_a), and the interaction enthalpy (ΔH).

RESULTS

Secondary Structure and Structural Stability. The CD spectrum of apo-N-HsCen2 strongly suggests that, even in the absence of bound metal ions, the domain has a significant content of secondary structure. The spectrum is characteristic for helical-rich proteins, with two minima at 208 and 222 nm and a maximum at 192 nm (Figure 2). Using several analysis programs and the protein basis sets available on the DICHROWEB web site (*25*), we obtained a consistent prediction of 33% α-helix content and a rather high content of β-sheet (18%). This is similar to the observations made on integral EF-hand proteins or their isolated domains

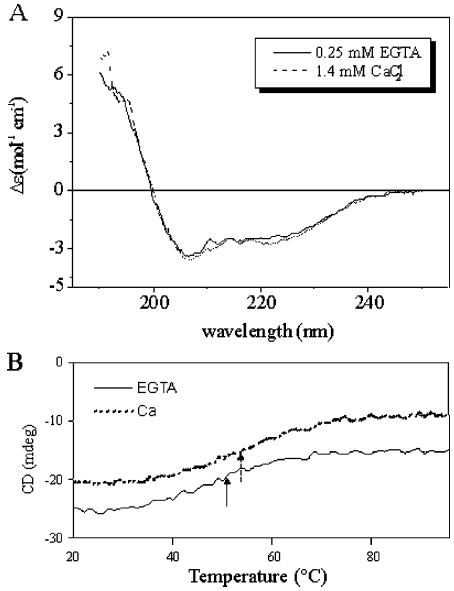

FIGURE 2: Secondary structure and thermal denaturation. (A) CD spectra at 20 °C of N-HsCen2 in the presence (1.4 mM $CaCl_2$) or the absence (0.25 mM EGTA) of calcium. Protein samples (10 μM) were dissolved in 1 mM MOPS buffer and 0.4 mM NaCl. (B) Thermal denaturation curves of N-HsCen2 in the presence and the absence of calcium, obtained by monitoring the ellipticity at 222 nm. The vertical arrows indicate the position of the mid-temperature of denaturation.

(*17*, *18*, *26*, *27*). Ca^{2+} ions do not change significantly the CD spectrum, suggesting that the secondary structure and the global folding of the domain are not perturbed by the presence of a large excess of metal cations.

The thermal denaturation curve of N-HsCen2 is highly reversible and reveals a cooperative transition at 50 and 54 °C for apo and holo forms, respectively (Figure 2). Observation of a cooperative thermal unfolding of the apo form of N-HsCen2 is in contrast with the behavior of the apo-C-terminal lobe, which shows a progressive decrease of the ellipticity with no apparent transition, reflecting a highly dynamic structural organization. The N-terminal lobe is therefore more compact and better structured even in the absence of Ca^{2+}. CD experiments performed on N-HsCen1 give very close values for secondary structure content and stability parameters.

Solution Structure of Apo-N-HsCen2. The ($^{15}N-^{1}H$)-HSQC spectrum of the apo-N-HsCen2 (Figure 3) is well dispersed (more than 3 ppm in the proton dimension) and contains the expected number of cross-peaks, suggesting that the EF-hand domain has a unique, persistent, and well-defined tertiary structure in the absence of bound metal ions. The standard approach for sequential assignment of the protein spectrum, based on 2D (*21*) and 3D (*28*) NMR experiments, enabled us to assign the backbone and the majority of the side chain resonances in the protein fragment from R18 to S98. The spin systems represented by the framed cross-peaks in Figure 3 exhibit random coil chemical shifts (for example, the amide protons resonate between 7.8 and 8.4 ppm) and provide only a few NOE interactions. They correspond to the first 17 residues and will remain unassigned. The average line width of the cross-peaks is consistent with a largely monomeric form of the domain. A notable difference is represented by the downfield-shifted Gly46 and Gly82 cross-peaks, which correspond to the amide group in the residues located at the sixth position (G^6) of the Ca^{2+} binding loop in EF-hands I and II, respectively. Their unusual chemical shift provides a spectroscopic probe for the formation of the typical intraloop hydrogen bond between this amide proton and one carboxyl oxygen of the D^1 residue in position 1 of the loop (*29*). Initially thought to be a signature of the bound conformation, its observation in some Ca^{2+}-free EF-hands (*30*, *31*) demonstrated that this hydrogen bond may also exist in the absence of metal binding. The broadening in the proton dimension of Gly46 and Gly82 peaks (and to a lesser extent of the neighboring Thr45 and Thr81) suggests that these particular fragments exhibit local conformational exchanges in the intermediate regime on the NMR time scale.

In accord with the high sequence identity with N-HsCen2 (76%), N-HsCen1 shows very similar NMR spectra and NOE connectivity patterns. However, the significant temperature-dependent general broadening of the cross-peaks suggests that this domain is in dynamic equilibrium between several exchanging conformations. The spectra were therefore acquired at 298 K, where the peaks become significantly sharper.

The NMR experimental data, including the secondary structure delimitation and different conformational restraints (1159 distances, 36 hydrogen bonds, and 50 dihedral angles), were used to calculate an ensemble of 20 molecules, representative for the solution structure of the N-HsCen2. The final structures were selected according to the low potential energy, as well as the agreement with the stereochemical ideal parameters and experimental data (Table 1). Analysis of the ensemble main chain dihedral angles indicates that 97.1% of the ϕ and ψ angles fall into the allowed region of the Ramachandran plot. Among the 3% of the residues falling in the disallowed region of the plot, the majority belong to the unstructured N-terminal segment or to the linker between the two EF-hand motifs (Phe62). Figure 4 illustrates the calculated structures using various representations, including the superimposed backbone of the protein ensemble, the simplified ribbon drawing of the main chain fold, and the hydrophobic core. Fragment 27−98 of apo-N-HsCen2 is well organized, with two characteristic EF-hand motifs linked via a short antiparallel β-sheet (47−49 and 83−85). The four α-helices (A, 27−40; B, 50−61; C, 68−76; D, 86−98), comprising 48% of the residues, show a regular and persistent structure with the characteristic short- and medium-range interproton NOEs. As in the apo structure of the CaM N-terminal domain (*32*), helix C is more isolated from the other closely packed helices, resulting in a poorer regularity and a less defined tertiary position.

The tertiary structure is characterized by an almost antiparallel arrangement of the four helices similar to that of other apo-EF-hand domains, including the N-terminal half of CaM (*32*), TnC (*33*), and CaVP (*30*). The mean interhelical angles, calculated with the Interhlx software (K. Yap, University of Toronto), are A/B 152° and C/D 141° (Table 2). These values fall in the upper range encountered in the structures of calcium-free domains (*30*, *32*−*34*), allowing us to classify apo-N-HsCen2 as one of the most compact. Global structure comparison of N-HsCen2 shows the highest similarity (rmsd = 1.48 Å) with the N-terminal lobe of CaVP (PDB file 1J7R), an EF-hand domain that lost the metal binding capacity and performs its cellular function in the

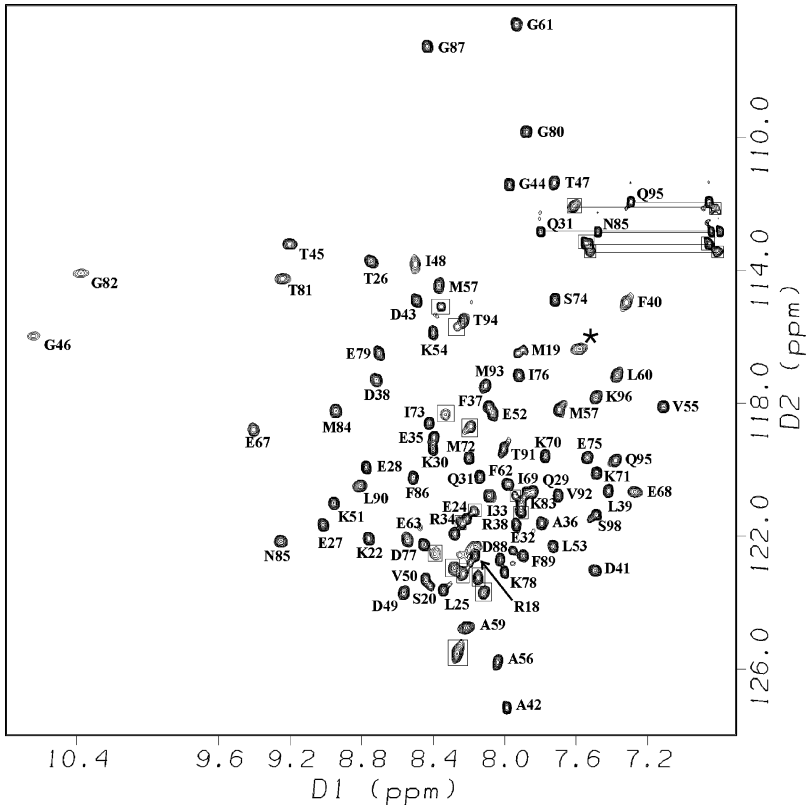

FIGURE 3: (^{1}H−^{15}N)-HSQC spectrum of apo-N-HsCen2. The protein sample (1.2 mM) was dissolved in 20 mM Tris-d_{11} buffer, pH 6.5, and 100 mM NaCl, and the spectrum was recorded at 500 MHz and 308 K. The individual cross-peaks represent amide groups of non-proline residues, while the paired peaks connected by a horizontal line correspond to side chain amino groups in Asn and Gln amino acids. The assignment is indicated by the type and the number of the residue. Unassigned peaks, corresponding to the fragment Met1−Lys17, are boxed. The asterisk indicates a folded cross-peak corresponding to a Lys side chain.

Table 1: Experimental Restraints and Structural Statistics of the Final 20 Structures

total no. of distance restraints	1159
intraresidue	453 (39%)
sequential ($\|i-j\|=1$)	366 (32%)
medium range ($1<\|i-j\|<5$)	183 (16%)
long range ($\|i-j\|\geq 5$)	157 (14%)
no. of restrained hydrogen bonds	36
no. of dihedral angle restraints (ϕ,ψ)	50
violation statistics	
violations per structure (>0.5 Å)	none
dihedral angle restrains violations (> 10°)	none
rmsd of NOE upper violation (Å)	0.027
rmsd of NOE lower violation (Å)	0.025
max NOE upper violation (Å)	0.33
max NOE lower violation (Å)	0.32
max dihedral angle violation (deg)	5
average rmsd (Å) from average structure	
residues 27−40, 47−61, 68−76, 83−98[a]	0.64 ± 0.02
EF-hand I[a]	0.57 ± 0.02
EF-hand II[a]	0.71 ± 0.03
helix A[a]	0.52 ± 0.03
helix B[a]	0.64 ± 0.03
helix C[a]	0.84 ± 0.04
helix D[a]	0.63 ± 0.03
all heavy atoms (27−98)	1.57 ± 0.04
ensemble Ramachandran plot	
residues in most favored regions (%)	69.6
residues in additionally allowed regions (%)	24.6
residues in generously allowed regions (%)	2.9
residues in disallowed regions (%)	2.9

[a] Backbone atoms (N, C′, and C$^\alpha$).

apo form (*30*). Superposition to other Ca^{2+}-free structures of CaM or TnC results in significantly higher rmsd values (from 2.49 to 3.47 Å), in agreement with the above analysis of the interhelix angles.

Many of the residues composing the hydrophobic core (three Phe, three Ile, two Leu, and five Met) are conserved or conservatively substituted in other centrins or members of the CaM family. The entrance into the internal core is closed by a hydrophobic cap formed by Met97 and Phe62. It is worth noting that helix C participation to the hydrophobic packing is reduced to only Met72, and this may explain the poorer definition of this segment in the structure. Two of the N-terminal lobe mutations affecting the biological function of Cdc31 (the yeast centrin) correspond to Leu53 and Met72 of HsCen2 (*35*). According to the present structural analysis, substitution of these alkyl side chains may destabilize the side chain packing in the hydrophobic core of the domain and decrease the overall protein stability.

N-HsCen2 contains many charged side chains (17 Glu + Asp and 18 Arg + Lys), unequally distributed on the molecular surface, as may be seen from the electrostatic potential calculated for well-defined fragment 27−98 (Figure 4D). A large negative surface is defined by the external side of A and B helices, and this is neighbored by a hydrophobic surface (including V50, I69, and I73) surrounded by several positive charges from residues in helices B an C (Figure 4D, left). It is notable that four of the positively charged residues in this area are well conserved in human centrins (K65, K66, K70, and K71; see Figure 1) but are not present in CaM or TnC.

In the absence of spectral assignment for a large part of the N-terminal fragment (from M1 to K17), the structure of this segment remains undetermined (Figure 4A). Under the

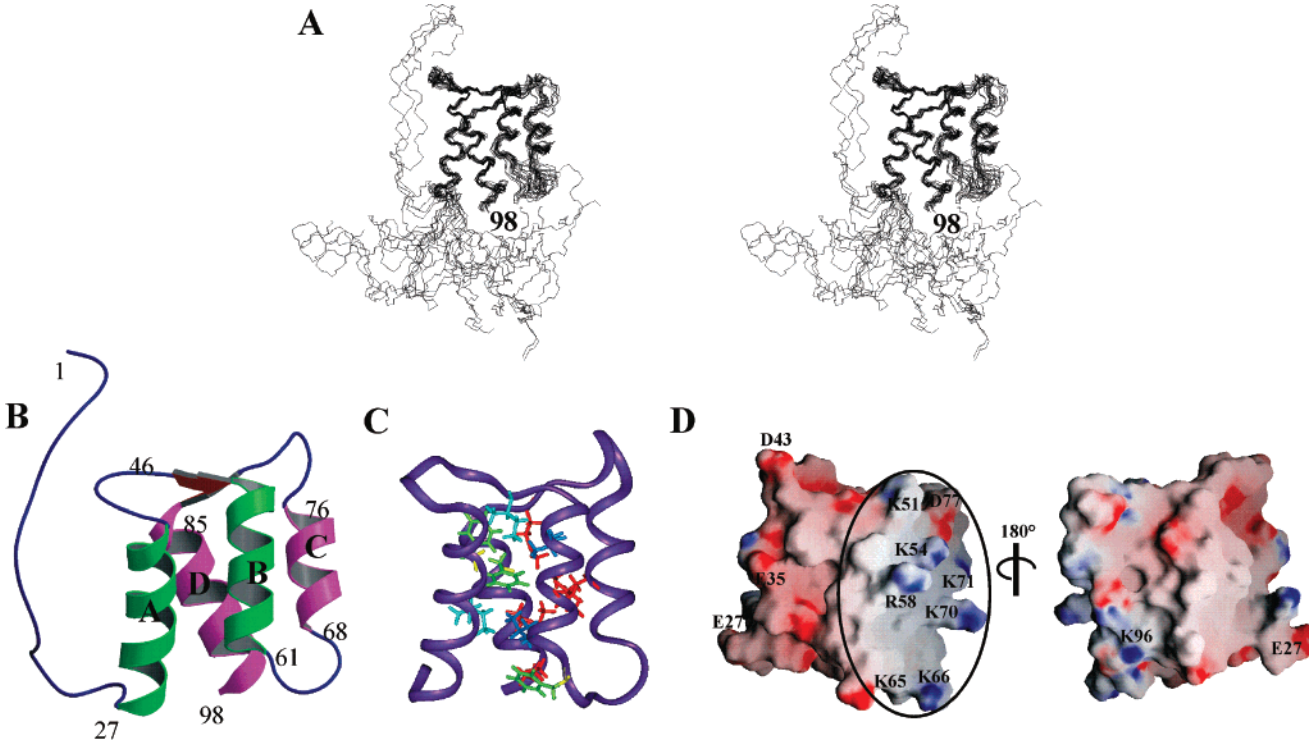

FIGURE 4: Overview of the solution structure of N-HsCen2. (A) Stereoview of the backbone superposition of the 20 NMR-derived structures, optimized to minimize the rmsd between main chain atoms (N, C′, C^{α}) within regular secondary structure elements. (B) Ribbon representation of the main chain fold in a representative structure of the ensemble. The image was drawn with MOLSCRIPT (*46*) and Raster 3D (*47*) software. (C) Stick representation of the side chains constituting the hydrophobic core. The backbone, in the same orientation as in panel B, is reduced to fragment 25−98. Phe are in green, Ile are in cyan, Leu are in blue, and Met are in red. (D) GRASP representation of the electrostatic potential, calculated at the molecular surface of the representative structure of N-HsCen2. Negative and positive potential values are gradually represented in red and blue colors, respectively. The left view is as in panel B, while the right view is rotated by 180°.

Table 2: Interhelical Angles and Distances between Midpoints of the Helices in the Final 20 Structures

	average angle (deg)	average distance (Å)
A/B	152 ± 4	12.0 ± 0.4
C/D	141 ± 5	12.3 ± 0.5
A/C	−50 ± 7	19.0 ± 0.4
A/D	148 ± 3	12.1 ± 0.3
B/C	155 ± 6	11.4 ± 0.4
B/D	−30 ± 5	14.3 ± 0.6

chemical constraints and physical force field used for the structure calculations, the corresponding main chain populates a large conformational space around its anchoring point. Among these conformations, only a subset, represented here by three members, where the flexible chains are antiparallel to the A helix, should be relevant for the integral protein. The other conformers are sterically forbidden by the presence of the E helix and the rest of the C-terminal domain.

A *Model for N-HsCen1*. Analysis of the NMR spectra of apo-N-HsCen1 at 298 K revealed many common spectral characteristics with N-HsCen2, including chemical shift values and distance-dependent NOE interactions. The reduced number of experimental information, due to a poorer quality of NMR spectra, precluded a structure calculation under NMR restraints, but the high sequence identity of the N-terminal domains (82% for the well-structured portion) enabled us to obtain a model by homology building. Analysis of the energy-minimized model shows that N-HsCen1 is structurally very similar to N-HsCen2 and that the surface electrostatic potential conserves the positive cavity delineated by the B and C helices.

Ca^{2+} Binding. The relatively high protein concentrations used in NMR experiments make possible the titration of low-affinity calcium binding sites. We started with a ^{15}N uniformly labeled N-HsCen2 solution (0.8 mM) in the apo state and progressively increased the Ca^{2+} content by adding small aliquots of a Ca^{2+} stock solution into the NMR tube. No significant pH change was observed during the experiment. On the basis of the spectral assignment of the apo form, and recording 1D and 2D ^{15}N-HSQC spectra along the titration, we monitored the calcium-induced proton and nitrogen chemical shift changes for a large part of the residues. Selected peaks in the HSQC spectrum move progressively, demonstrating that the N-terminal domain has the capacity to bind the divalent cation and that the bound and free protein forms are in a fast exchange regime. The observed chemical shifts are population-weighted average values between resonances in unbound and bound species. The maximum spectral perturbations, estimated by the combined (^{1}H and ^{15}N) chemical shift changes of the amide groups, are represented along the protein sequence in Figure 5A. It is readily apparent that the number and amplitude of the spectral perturbations are significantly larger in the first EF-hand motif (there are two times more peaks showing a combined chemical shift change larger than 0.2 ppm in EF-hand I relative to EF-hand II). The calcium dependence of the normalized chemical shift changes is very similar in the two motifs (Figure 5B), suggesting that the conformational changes are induced simultaneously by the same binding event. Indeed, the best fit of the experimental data could be obtained only by using a one-site binding model for all of

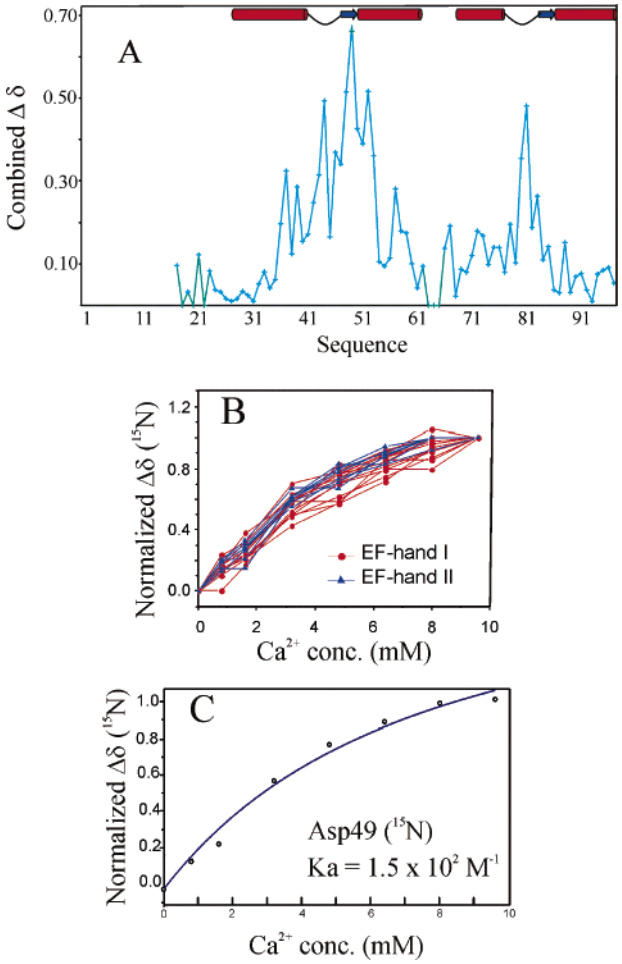

FIGURE 5: Calcium titration of N-HsCen2. (A) Combined chemical shift changes [$\Delta\delta(^1H) + \Delta\delta(^{15}N)/5$] observed at the end of the calcium titration along the sequence of N-HsCen2. The secondary structure elements are schematically shown on the top of the panel. (B) Normalized ^{15}N chemical shift changes upon Ca^{2+} titration for 14 residues in EF-hand I and 7 residues in EF-hand II which show a final combined chemical shift change larger than 0.2 ppm. (C) Example of the best fit of the experimental data, using a single-site binding model, corresponding to residue D49.

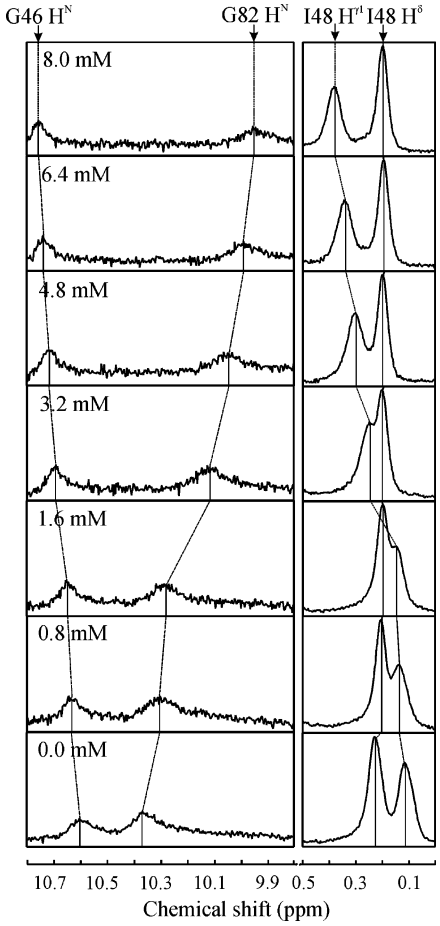

FIGURE 6: Proton spectral probes for the calcium-sensitive conformational changes. Spectral features including the proton resonances of amide G46, amide G82, and the side chain of Ile48 along the calcium titration. The sample (0.8 mM) was obtained by dissolving the lyophilized protein into deuterated Tris buffer (20 mM, pH 6.6) and 100 mM NaCl, and the spectra were recorded at 500 MHz and 308 K.

the sensitive spectral probes (Figure 5C). The mean optimized binding constant is 1.4×10^2 M^{-1}, about 3 orders of magnitude lower than in the C-terminal half of HsCen2 (*14*). Taking into account the low cellular calcium concentrations ($10^{-7}-10^{-5}$ M) this low affinity means that the physiological state of the N-terminal half of HsCen2 is the free state, with the structure determined in this work. The calcium-dependent spectral changes (Figure 5A) are mainly localized to the binding loop residues, and their distribution suggests that the first EF-hand is more sensitive. Similar conclusions were drawn from the study of the N-terminal domain of HsCen1, except that the binding affinity is 1 order of magnitude larger (2.9×10^3 M^{-1}). Sequence analysis of the two Ca^{2+} binding loops in HsCen1 and HsCen2 does not uncover major side chain differences relative to the canonical binding sequence (*36*), which would explain the very low affinity of the N-terminal half. The sequence of the second loop is somewhat more distant from the optimum (for instance, the presence of an Asp residue in the 12th position, usually represented by a Glu), predicting a weaker binding site, in agreement with the above suggestion. Other factors could contribute as well to the decreased affinity, one of them being the positive surface charges around the metal binding sites (*37*, *38*), particularly Lys51 and Lys83. As we noted earlier, the N-terminal domains of HsCen1 and HsCen2 have a distinctive high pH_i and exhibit clusters of positive side chains (Figure 4D) that may induce a decreased association rate for positive metal ions.

Ca^{2+}-Induced Conformational Changes. As we noted before, observation of the low-field amide resonances of Gly46 and Gly82 (10.61 and 10.37 ppm, respectively) at the beginning of the titration (Figure 3) indicates that the intraloop hydrogen bonds with the D^1 carboxyl oxygen are formed even in the absence of the bound calcium. Ca^{2+} titration into the protein solution produces opposite effects on the two Gly resonances (Figure 6): the peak from Gly46 is slightly low field shifted and becomes sharper, while the peak of Gly82 is shifted to a higher field and broadens (it represents the largest chemical shift change in the second binding loop). This observation is compatible with the binding of calcium to EF-hand I and a consequent reinforcement of the hydrogen bond $CO(D^1)-HN(G^6)$ in this motif. Simultaneously, the corresponding hydrogen bond of the second binding loop seems to be weakened and more fluctuating. The structural changes observed in EF-hand II could be explained by metal binding to the first motif and propagation of the induced perturbations through the short

antiparallel β-sheet constituting the "EFβ-scaffold" (*39*). This hypothesis is also supported by the analysis of calcium-dependent changes of a pivotal residue in this platform, occupying the eighth position in the binding loop (Ile48 and Met84). The amide ^{15}N chemical shift of these residues is compatible with the average values observed for the apo-EF-hand sites (*40*). Unfortunately, the peak corresponding to Ile48 broadens early in the titration process, and thus its holo chemical shift remains unknown. In contrast, the amide resonance of Met84 could be followed until the end of the titration, when its chemical shift (119.5 ppm) is still within the range observed for apo forms, suggesting that the second binding site remains empty.

In EF-hand proteins, the $H^{\alpha}-C^{\alpha}-C^{\beta}-H^{\beta}$ torsion angle of the hydrophobic residue in position 8 is in a trans conformation in sites II and IV and does not change between apo and holo forms (*40*), while in sites I and III this angle changes from gauche(−) to trans upon Ca^{2+} binding. In accord with these observations, Ca^{2+} binding to the first binding loop of N-HsCen2 is reflected in a large highfield shift (∼0.3 ppm) of the $H^{\gamma 11}/H^{\gamma 12}$ resonance of Ile48 (Figure 6). As this residue is situated in the center of the compact hydrophobic core, its conformational changes may be easily transmitted to side chains of the other binding loop.

The chemical shift of D^1 is another sensitive probe for the calcium-induced conformational change: whenever a Phe residue is present in position −4, one of the H^{β} protons in D^1 is highfield shifted by more than 1 ppm in the ion-bound conformation (*41*). In the case of N-HsCen2, only Asp41 constitutes such a probe, and indeed in the apo form, the H^{β} chemical shifts (2.14/2.77 ppm) are closer to characteristic values for unbound sites. At the end of the titration, the corresponding chemical shifts are only slightly changed (1.99/2.68 ppm), suggesting that the tertiary conformation (particularly the A/B interhelix angle) remains similar to the closed conformation. Overall, the observed titration features, including the spectroscopic probes and the long-range NOEs, suggest that the Ca^{2+} binding to the first EF-hand induces local structural perturbations in both binding loops but maintains the closed tertiary conformation of the whole domain.

Binding Properties of the N-Terminal Fragment. One of the sources of sequence diversity among the centrin N-terminal domains is related to the different length and the variable composition of the segment preceding the first EF-hand motif (Figure 1). This fragment is absent in CaM and shorter in TnC, where it forms an additional α-helix (called the N helix) structurally linked to A and D helices. The sequence of the N-fragment in HsCen2 has many positively charged residues (four Lys and two Arg) and exhibits a very flexible structure. Nevertheless, recent experiments conducted in our laboratory, using a truncated variant of HsCen2 lacking the first 25 residues (Δ25HsCen2), suggested that the N-fragment may play a role in the self-association of centrin molecules and, therefore, contributes to the regulation of the centrosomes' and basal bodies' structural components (*42*). To assess this hypothesis, we synthesized an 18-residue peptide spanning the sequence F5−K22 of HsCen2 (N-18) and explored its interaction properties with various constructs derived from the wild-type protein.

Titration of a 250 μM N-18 solution into the buffer alone shows no significant heat exchange (not shown), indicating that the peptide does not form dissociable oligomers and that the heat of dilution is negligible. As shown by the CD experiments, the peptide alone is not structured in solution (data not shown). When the apo form of the C-HsCen2 (at 50 μM) is titrated by the peptide, a series of negative heat exchange peaks with decreasing intensity were recorded, reflecting an exothermic intermolecular interaction (Figure 7A). Peak integration and fitting to a one-site interaction model give an affinity on the order of 10^5 M^{-1} (8.4×10^4 M^{-1}, mean of two experiments), a moderate enthalpy (−3.5 kcal/mol, mean value), and a stoichiometry of 0.46. The corresponding free energy of the interaction is −6.8 kcal/mol, while the entropic component is $T\Delta S = +3.3$ kcal/mol, meaning that the interaction is driven by both enthalpic and entropic contributions. The positive entropy change should originate from the decrease in hydration of the two molecules (mostly of the positively charged peptide) upon complex formation with the consequent increase of the solvent entropy. Binding of the N-18 peptide to the C-terminal half of HsCen2 does not significantly change in the presence of 1 mM Ca^{2+} (data not shown).

It is interesting to note that a longer construct representing the C-terminal domain of HsCen2 (named LC-HsCen2: M84−Y172), including the D helix (that normally belongs to the N-terminal half) (*14*), shows no significant binding to the peptide (Figure 7B). As shown by the solution structure of this construct, the D helix lies over the hydrophobic cavity created by the E−H α-helices in the presence of Ca^{2+} ions, in a similar geometry to that of a target molecule. This observation suggests that the binding area of N-18 to C-HsCen2 is close to the target binding site of the centrin molecule and may be modulated by the presence of target molecules.

Finally, we studied the interaction with Δ25HsCen2, a variant that shows a decreased self-assembly tendency (*42*). N-18 also binds to this variant with a lower affinity (Figure 7C). The stoichiometry is again close to 0.5, suggesting that a peptide molecule binds to a dimer formed by two protein molecules. A similar model involving one N-terminal and several C-terminal domains emerged from the similar experiments using the whole N-terminal domain (*42*). To check the specificity of N-18 for the C-terminal half of HsCen2, we also performed ITC binding experiments using the bovine calmodulin. Experiments conducted in the same conditions as with centrin constructs showed no detectable interaction between N-18 and CaM (data not shown), suggesting that the sequence of the C-terminal domain is also an important factor for binding.

DISCUSSION

The solution structure of the N-terminal domains of HsCen1 and HsCen2 in the absence of calcium is highly similar to the closed conformation of apo-EF-hand domains. As the calcium dissociation constant of these domains is at least 2 orders of magnitude higher than the average metal concentration in activated cells, this structure is relevant for the cell state of centrins. The similar denaturation properties of the isolated N-terminal domain and of the N-terminal half in the integral centrin reinforce the biological significance of the present results. Indeed, the transition temperature of the isolated N-terminal domain in the presence of Ca^{2+} (54 °C) corresponds to the first transition in the denaturation of the intact holo-HsCen2 (45 °C) that was associated with the

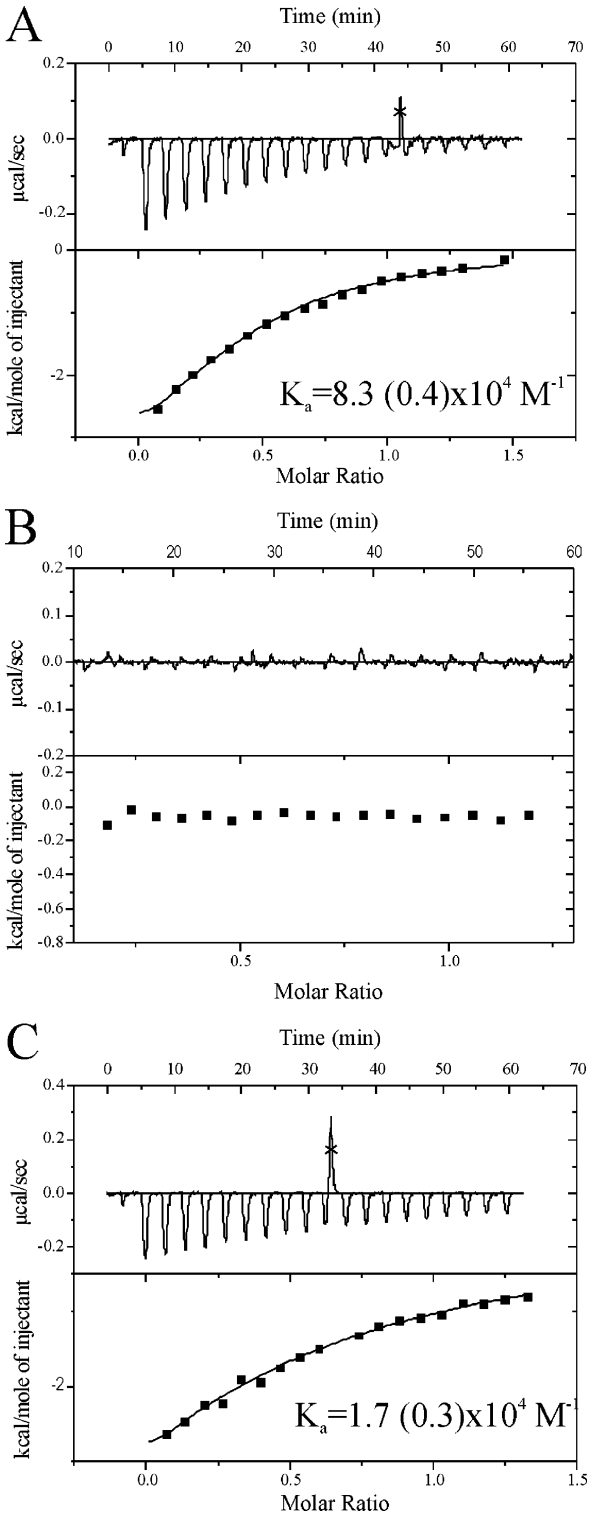

FIGURE 7: Calorimetric study of N-18 intermolecular interactions. (A) A solution of 250 μM N-18 (50 mM MOPS buffer, pH 6.8, 20 mM NaCl, no Ca^{2+}) was titrated into a 50 μM C-HsCen2 solution at 308 K using 15 μL automated injections. The heat exchange peaks (upper panel) were integrated and fitted to a one-site binding model (lower panel) to obtain the reaction stoichiometry ($n = 0.46$), the binding constant [$K_a = (9 \pm 1) \times 10^5$ M^{-1}], and the binding enthalpy ($\Delta H = -4.6 \pm 0.4$ kcal/mol). (B) Titration of the LC-HsCen2 (50 μM in 50 mM MOPS buffer, pH 6.8, 20 mM NaCl, 1 mM $CaCl_2$) by 250 μM N-18 at 308 K. (C) Titration of Δ25HsCen2 (50 μM in 50 mM MOPS buffer, pH 6.8, 20 mM NaCl, 1 mM $CaCl_2$) by N-18 at 308 K. The fitted thermodynamic parameters are $n = 0.47$, $K_a = (1.7 \pm 0.3) \times 10^4$ M^{-1}, and $\Delta H = -6.9$ kcal/mol.

N-terminal half (*17*). Further, the low Ca^{2+} binding affinity of N-HsCen2 is consistent with our previous results, which demonstrated that the physiologically significant metal binding sites of the integral protein are situated within the C-terminal domain of HsCen2 and are independent of millimolar concentrations of Mg^{2+} (*14*, *16*). Altogether, these observations strongly suggest that the closed structure, determined here for the isolated N-terminal domain, corresponds to the conformational state of the N-terminal half in the integral protein. Consequently, this domain is not able to expose a hydrophobic cavity that generally constitutes the binding site for target molecules (*43*). This conclusion is in agreement with previous observations on HsCen2 (*17*) or Cdc31 (*35*), suggesting that the N-lobe of these centrins is not critical for the heteromolecular interactions.

Nevertheless, the N-terminal domain, and particularly its basic flexible fragment, may play an active role in the self-assembly of centrin molecules within centrosomes and basal bodies (*26*, *42*). The electrostatic analysis of the three-dimensional structure revealed a well-defined cluster of basic residues surrounding a small hydrophobic area (Figure 4D) at the molecule surface, which may constitute a binding site to acidic regions of other molecules. Moreover, the present calorimetric data confirmed the hypothesis of an active role played by the first 25 residues in the self-association of centrins (*42*). The binding stoichiometry observed here suggests that the structural basis of this process is a complex where two C-terminal domains interact to create a negative binding site for the positively charged N-terminal fragment of a third centrin molecule. It is worth noting that the three molecular interaction mode proposed here may be related to the calcium-dependent reticulate aspect of the algal centrins organization, revealed by electron microscopy (*26*, *44*). Interestingly, as suggested by the experiments using a particular construct (LC-HsCen2), the homomolecular interactions could be modulated by heteromolecules that usually bind with stronger affinity to the C-terminal hydrophobic cavity. Therefore, an equilibrium may exist between the self-association tendency of centrins and the interaction with specific target proteins that would depend on the relative affinity, the Ca^{2+} local concentration, and other physicochemical parameters in a particular cell compartment (*45*). A better molecular and energetic description of this equilibrium should be very useful for the understanding of the regulatory role of centrin in the structural dynamics of centrosomes and basal bodies.

ACKNOWLEDGMENT

We thank Michel Bornens for the clone of HsCen1, Latifa Ziani for participation in the initial phase of the project, and Damarys Loew for the mass spectrometry analysis.

REFERENCES

1. Salisbury, J. L., Baron, A., Surek, B., and Melkonian, M. (1984) Striated flagellar roots: isolation and partial characterization of a calcium-modulated contractile organelle, *J. Cell Biol. 99*, 962−970.
2. Geimer, S., and Melkonian, M. (2004) The ultrastructure of the *Chlamydomonas reinhardtii* basal apparatus: identification of an early marker of radial asymmetry inherent in the basal body, *J. Cell Sci. 117*, 2663−2674.
3. Paoletti, A., Moudjou, M., Paintrand, M., Salisbury, J. L., and Bornens, M. (1996) Most of centrin in animal cells is not

centrosome-associated and centrosomal centrin is confined to the distal lumen of centrioles, *J. Cell Sci. 109*, 3089−3102.
4. Salisbury, J. L., Suino, K. M., Busby, R., and Springett, M. (2002) Centrin-2 is required for centriole duplication in mammalian cells, *Curr. Biol. 12*, 1287−1292.
5. Paoletti, A., Bordes, N., Haddad, R., Schwartz, C. L., Chang, F., and Bornens, M. (2003) Fission yeast cdc31p is a component of the half-bridge and controls SPB duplication, *Mol. Biol. Cell 14*, 2793−2808.
6. Wright, R. L., Salisbury, J., and Jarvik, J. W. (1985) A nucleus-basal body connector in *Chlamydomonas reinhardtii* that may function in basal body localization or segregation, *J. Cell Biol. 101*, 1903−1912.
7. McFadden, G. I., Schulze, D., Surek, B., Salisbury, J. L., and Melkonian, M. (1987) Basal body reorientation mediated by Ca^{2+}-modulated contractile protein, *J. Cell Biol. 105*, 903−912.
8. Sanders, M. A., and Salisbury, J. L. (1994) Centrin plays an essential role in microtubule severing during flagellar excision in *Chlamydomonas reinhardtii*, *J. Cell Biol. 124*, 795−805.
9. Araki, M., Masutani, C., Takemura, M., Uchida, A., Sugasawa, K., Kondoh, J., Ohkuma, Y., and Hanaoka, F. (2001) Centrosome protein centrin 2/caltractin 1 is part of the *Xeroderma pigmentosum* group C complex that initiates global genome nucleotide excision repair, *J. Biol. Chem. 276*, 18665−18672.
10. Fischer, T., Rodriguez-Navarro, S., Pereira, G., Racz, A., Schiebel, E., and Hurt, E. (2004) Yeast centrin Cdc31 is linked to the nuclear mRNA export machinery, *Nat. Cell Biol. 6*, 840−848.
11. Gonda, K., Yoshida, A., Oami, K., and Takahashi, M. (2004) Centrin is essential for the activity of the ciliary reversal-coupled voltage-gated Ca^{2+} channels, *Biochem. Biophys. Res. Commun. 323*, 891−897.
12. Gavet, O., Alvarez, C., Gaspar, P., and Bornens, M. (2003) Centrin4p, a novel mammalian centrin specifically expressed in ciliated cells, *Mol. Biol. Cell 14*, 1818−1834.
13. Veeraraghavan, S., Fagan, P. A., Hu, H., Lee, V., Harper, J. F., Bessie, H., and Chazin, W. J. (2002) Structural independence of the two EF-hand domains of caltractin, *J. Biol. Chem. 277*, 28564−28571.
14. Matei, E., Miron, S., Blouquit, Y., Duchambon, P., Durussel, I., Cox, J. A., and Craescu, C. T. (2003) The C-terminal half of human centrin 2 behaves like a regulatory EF-hand domain, *Biochemistry 42*, 1439−1450.
15. Weber, C., Lee, V. D., Chazin, W. J., and Huang, B. (1994) High level expression in *Escherichia coli* and characterization of the EF-hand calcium-binding protein caltractin, *J. Biol. Chem. 269*, 15795−15802.
16. Durussel, I., Blouquit, Y., Middendorp, S., Craescu, C. T., and Cox, J. A. (2000) Cation- and peptide-binding properties of human centrin 2, *FEBS Lett. 472*, 208−212.
17. Popescu, A., Miron, S., Blouquit, Y., Duchambon, P., and Craescu, C. T. (2003) *Xeroderma pigmentosum* group C protein possesses a high affinity binding site for human centrin 2 and calmodulin, *J. Biol. Chem. 278*, 40252−40261.
18. Hu, H., Sheehan, J. H., and Chazin, W. J. (2004) The mode of action of centrin: binding of Ca^{2+} and a peptide fragment of Kar1p to the C-terminal domain, *J. Biol. Chem. 279*, 50895−50903.
19. Cox, J. A., Durussel, I., Firanescu, C., Blouquit, Y., Duchambon, P., and Craescu, C. T. (2005) Calcium and magnesium binding to human centrin 3 and interaction with target peptides, *Biochemistry 44*, 840−850.
20. Munier, H., Gilles, A. M., Glaser, P., Krin, E., Danchin, A., Sarfati, R., and Barzu, O. (1991) Isolation and characterization of catalytic and calmodulin-binding domains of *Bordetella pertussis* adenylate cyclase, *Eur. J. Biochem. 196*, 469−474.
21. Wüthrich, K. (1986) *NMR of Proteins and Nucleic Acids*, Wiley, New York.
22. Nilges, M., Clore, G. M., and Gronenborn, A. M. (1988) Determination of three-dimensional structures of proteins from interproton distance data by hybrid distance geometry-dynamical simulated annealing calculations, *FEBS Lett. 229*, 317−324.
23. Laskowski, R. A., Rullmann, J., Antoon, C., MacArthur, M. W., Kaptein, R., and Thornton, J. M. (1996) AQUA and PROCHECK-NMR: Programs for checking the quality of protein structures solved by NMR, *J. Biomol. NMR 8*, 477−486.
24. Nicholls, A., Sharp, K. A., and Honig, B. (1991) Protein folding and association: insights from the interfacial and thermodynamic properties of hydrocarbons, *Proteins: Struct., Funct., Genet. 11*, 281−296.
25. Lobley, A., Whitmore, L., and Wallace, B. A. (2002) DICHROWEB: an interactive website for the analysis of protein secondary structure from circular dichroism spectra, *Bioinformatics 18*, 211−212.
26. Wiech, H., Geier, B. M., Paschke, T., Spang, A., Grein, K., Steinkötter, J., Melkonian, M., and Schiebel, E. (1996) Characterization of green alga, yeast, and human centrins, *J. Biol. Chem. 271*, 22453−22461.
27. Martin, S. R., Lu, A. Q., Xiao, J., Kleinjung, J., Beckingham, K., and Bayley, P. M. (1999) Conformational and metal-bindding properties of androcam, a testis-specific, calmodulin-related protein from *Drosophila*, *Protein Sci. 8*, 2444−2454.
28. Cavanagh, J., Fairbrother, W., J., Palmer, A., G., III, and Skelton, N., J. (1996) *Protein NMR Spectroscopy. Principles and Practice*, Academic Press, San Diego.
29. McPhalen, C. A., Strynadka, N. C. J., and James, M. N. G. (1991) Calcium-binding sites in proteins: a structural perspective, *Adv. Protein Chem. 42*, 77−144.
30. Théret, I., Baladi, S., Cox, J. A., Gallay, J., Sakamoto, H., and Craescu, C. T. (2001) Solution structure and backbone dynamics of the defunct domain of calcium vector protein, *Biochemistry 40*, 13888−13897.
31. Rabah, G., Popescu, R., Cox, J. A., Engelborghs, Y., and Craescu, C. T. (2005) Solution structure and internal dynamics of NSCP, a compact calcium-binding protein, *FEBS J. 272*, 2022−2036.
32. Zhang, M., Tanaka, T., and Ikura, M. (1995) Calcium-induced conformational transition revealed by the solution structure of apo calmodulin, *Nat. Struct. Biol. 2*, 758−767.
33. Gagné, S. M., Tsuda, S., Li, M. X., Smillie, L. B., and Sykes, B. D. (1995) Structures of the troponin C regulatory domains in the apo and calcium-saturated states, *Nat. Struct. Biol. 2*, 784−789.
34. Kilby, P. M., Van Eldik, L. J., and Roberts, G. C. K. (1996) The solution structure of the bovine S100B protein dimer in the calcium-free state, *Structure 4*, 1041−1052.
35. Ivanovska, I., and Rose, M. D. (2001) Fine structure analysis of the yeast centrin, Cdc31p, identifies residues specific for cell morphology and spindle pole body duplication, *Genetics 157*, 503−518.
36. Falke, J. J., Drake, S. K., Hazard, A. L., and Peersen, O. B. (1994) Molecular tuning of ion binding to calcium signaling proteins, *Q. Rev. Biophys. 27*, 219−290.
37. Linse, S., Brodin, P., Johansson, C., Thulin, E., Grunström, T., and Forsèn, S. (1988) The role of protein surface charges in ion binding, *Nature 335*, 651−652.
38. Martin, S. R., Linse, S., Johansson, C., Bayley, P. M., and Forsen, S. (1990) Protein surface charges and Ca^{2+} binding to individual sites in calbindin D_{9k}: stopped-flow studies, *Biochemistry 29*, 4188−4193.
39. Grabarek, Z. (2005) Structure of a trapped intermediate of calmodulin: calcium regulation of EF-hand proteins from a new perspective, *J. Mol. Biol. 346*, 1351−1366.
40. Biekofsky, R. R., Martin, S. R., Browne, J. P., Bayley, P. M., and Feeney, J. (1998) Ca^{2+} coordination to backbone carbonyl oxygen atoms in calmodulin and other EF-hand proteins: ^{15}N chemical shifts as probes for monitoring individual-site Ca^{2+} coordination, *Biochemistry 37*, 7617−7629.
41. Atreya, H. S., and Chary, K. V. R. (2002) New chemical shift signature of bound calcium in EF-hand proteins, *Curr. Sci. 83*, 1240−1245.
42. Tourbez, M., Firanescu, C., Yang, A., Unipan, L., Duchambon, P., Blouquit, Y., and Craescu, C. T. (2004) Calcium-dependent self-assembly of human centrin 2, *J. Biol. Chem. 279*, 47672−47680.
43. Crivici, A., and Ikura, M. (1995) Molecular and structural basis of target recognition by calmodulin, *Annu. Rev. Biophys. Biomol. Struct. 24*, 85−116.
44. Salisbury, J. L. (1998) Roots, *J. Eukaryotic Microbiol. 45*, 28−32.
45. Salisbury, J. L. (2004) Centrosomes: Sfi1p and centrin unravel a structural riddle, *Curr. Biol. 14*, R27−R29.
46. Kraulis, P. (1991) MOLSCRIPT: a program to produce both detailed and schematic plots of protein structures, *J. Appl. Crystallogr. 24*, 946−950.
47. Merritt, E., A., and Bacon, D., J. (1977) Raster3D-photorealistic molecular graphics, *Methods Enzymol. 277*, 505−524.

BI051397S